Available online at www.sciencedirect.com
ScienceDirect
Journal of the European Ceramic Society 31 (2011) 2107–2117
www.elsevier.com/locate/jeurceramsoc

CuO as a sintering additive for $(Bi_{1/2}Na_{1/2})TiO_3$–$BaTiO_3$–$(K_{0.5}Na_{0.5})NbO_3$ lead-free piezoceramics

Wook Jo [a], Jean-Baptiste Ollagnier [a], Jong-Lo Park [b], Eva-Maria Anton [a], O-Jong Kwon [b], Chan Park [b,*], Hyun-Ho Seo [c], Jong-Sook Lee [c], Emre Erdem [d], Rüdiger-A. Eichel [d], Jürgen Rödel [a]

[a] *Institute of Materials Science, Technische Universität Darmstadt, Petersenstrasse 23, 64287 Darmstadt, Germany*
[b] *Department of Materials Science & Engineering, Seoul National University, Seoul 151-744, South Korea*
[c] *School of Materials Science & Engineering, Chonnam National University, Gwangju 500-757, South Korea*
[d] *Institut für Physikalische Chemie I, Albertstr. 21, Universität Freiburg, Germany*

Received 4 October 2010; received in revised form 25 April 2011; accepted 7 May 2011
Available online 31 May 2011

Abstract

CuO as a sintering additive was utilized to explore a low-temperature sintering of $0.92(Bi_{1/2}Na_{1/2})TiO_3$–$0.06BaTiO_3$–$0.02(K_{0.5}Na_{0.5})NbO_3$ lead-free piezoceramic which has shown a promise for actuator applications due to its large strain. The sintering temperature guaranteeing the relative density of greater than 98% is drastically decreased with CuO addition, and saturates at a temperature as low as ~930 °C when the addition level exceeds *ca.* 1 mol.%. Two distinguished features induced by the addition of CuO were noted. Firstly, the initially existing two-phase mixture gradually evolves into a rhombohedral single phase with an extremely small non-cubic distortion. Secondly, a liquid phase induced by the addition of CuO causes an abnormal grain growth, which can be attributed to the grain boundary reentrant edge mechanism. Based on these two observations, it is concluded that the added CuO not only forms a liquid phase but also diffuses into the lattice. In the meantime, temperature dependent permittivity measurements both on unpoled and poled samples suggest that the phase stability of the system is greatly influenced by the addition of CuO. Polarization and strain hysteresis measurements relate the changes in the phase stability closely to the stabilization of ferroelectric order, as exemplified by a significant increase in both the remanent strain and polarization values. Electron paramagnetic resonance (EPR) spectroscopic analysis revealed that the stabilization of ferroelectric order originates from a significant amount of Cu^{2+} diffusing into the lattice on B-site. There, it acts as an acceptor and forms a defect dipole in association with a charge balancing oxygen vacancy.

Keywords: Lead-free piezoceramics; C. Dielectric properties; C. Piezoelectric properties; A. Grain growth; B. Spectroscopy

1. Introduction

In response to the increasing concerns and regulations on the use of toxic materials for electric and electronic devices, the search for innocuous materials with competitive functional properties has been one of the hottest pursuits in the field of materials science and engineering over the last two decades.[1–7] This is especially true for the piezoelectric community, since widely used piezoceramics are highly dependent upon the presence of lead (Pb) that is listed among the six toxic materials to be abolished as early as possible. In addition, the research activities are largely driven by the exponentially increasing demand on high performance piezoceramics, which are essential to realize the desired technological achievements for the next generations, *e.g.* energy-effective, miniaturized, and integrated.[8] With a couple of breakthroughs,[9,10] two important classes of lead-free piezoceramics, *i.e.* $(K_{0.5}Na_{0.5})NbO_3$ (KNN)- and $(Bi_{1/2}Na_{1/2})TiO_3$ (BNT)-based materials, are now considered as the most promising in replacing lead-containing piezoceramics.[3–6]

In the case of actuator applications, large displacements are often facilitated using multilayer technology, where a piezoceramic as an active component and electrodes as passive

* Corresponding author.
E-mail address: pchan@snu.ac.kr (C. Park).

0955-2219/$ – see front matter © 2011 Elsevier Ltd. All rights reserved.
doi:10.1016/j.jeurceramsoc.2011.05.008

ones are co-fired.[11] In this case, the total cost is significantly affected by the cost of the electrode material. Therefore, Ag/Pd alloys are utilized and their thermochemical reactions with the ubiquitous PZT have been studied[12] and recently also extended to include the reactions with BNT-based lead-free piezoceramics.[13] A significant cost reduction is feasible using copper as an electrode material.[11] More affordable electrode materials, however, hinge on a low sintering temperature, which should preferably lie below 1000 °C. Low temperature sintering has an additional advantage in the case of lead-free piezoceramics, because they normally contain highly volatile elements such as Na, K, and Bi. In the case of KNN-based materials, CuO as a sintering additive has been successfully utilized to bring the sintering temperature down to as low as ~950 °C.[14,15] However, beyond the reduction in sintering temperature, the doping with CuO as sintering additive is accompanied by a pronounced impact on defect structure owing to the formation of defect dipoles as well as on the piezoelectric properties.[16]

Recently, we reported that an electric-field-induced strain of as large as ~0.45% can be achieved in 0.96BNT–0.06$BaTiO_3$ (BT) ceramics, when a small amount of BNT is replaced by KNN.[17] The follow-up studies for the dependence of properties on composition[18] and temperature[19] revealed that the giant strain is a consequence of a polymorphic phase boundary (PPB) shifted to room temperature by the addition of KNN. In other words, the large strain originates from the fact that the inherently large poling strain of electrically induced low temperature phase is fully reflected in each unipolar cycle due to a 'depolarization' effect caused by a 'non-polar' high temperature phase at zero field.[20] This reversible transition between two polymorphs was clearly demonstrated by *in situ* transmission electron microscopy studies[21] as well as *in situ* high energy X-ray diffraction studies combined with *in situ* neutron diffraction.[22] Here, the initially assumed 'non-polar' high temperature phase[20] was identified as a ferroelectric tetragonal *P4bm* phase, the ferroelectricity of which is extremely weak due to the very small tetragonal distortion (c/a ~1.0003).[22,23]

In this study, we have conducted a low temperature sintering of 0.92BNT–0.06BT–0.02KNN[20] using CuO as a sintering additive to see if the material is suitable for the fabrication of multilayered structures. In the meantime, a possible alteration in the electrical properties due to an incorporation of Cu^{2+} ions into the lattice was checked in consideration of the fact that Cu^{2+} replacing the B-site ions in the ABO_3-type perovskite structure is a well-known acceptor.[24] Note that in the case of the lead-free systems that normally contain several volatile elements, it is highly possible that the added copper, though in excess, could diffuse into the lattice. In fact, it was reported in KNN that the effect of copper diffusing into the lattice is so pronounced that once sintered at above 1000 °C, where the distribution of Cu^{2+} incorporated into the lattice is expected to be more homogeneous, KNN exhibits the characteristic features that define a 'hard' piezoceramic with a significant aging characteristic[25] and increased mechanical quality factor.[26]

2. Experimental procedure

$0.92(Bi_{1/2}Na_{1/2})TiO_3$–$0.06BaTiO_3$–$0.02(K_{0.5}Na_{0.5})NbO_3$–$x$CuO (100$x$CuO, x in mole fraction) was prepared through solid oxide route with reagent grade oxides and carbonates from the commercial powder manufacturer (Alfa Aesar). Firstly, properly weighed 0CuO powder based on its stoichiometric formula was ball-milled with a planetary mill (Frisch) using ethanol as a milling medium and yttria-stabilized zirconia balls for 24 h. Dried powders were calcined in a covered alumina crucible at 900 °C for 3 h. Then, an excess amount of CuO in mol.% of 0, 0.1, 0.2, 0.4, 0.8, 1.0, 1.6, 2.0, 4.0, and 8.0 was introduced to the calcined 0CuO, and the mixed powders were ball-milled again in a planetary mill with the same conditions used for the initial milling step. The obtained powders of each composition were uniaxially shaped into pellets and compacted hydrostatically at 150 MPa. To find the temperature where the relative density determined by Archimedes method reaches ~98%, sintering was performed from 900 °C up to 1150 °C with about a 20 °C step, while the sintering time was kept constant at 3 h. The compositions will be abbreviated hereafter as 100xCuL or 100xCuH depending on the sintering temperature adopted. Any sintering temperature lower than 1150 °C was termed as L and 1150 °C as H. Specimens were heated up to each sintering temperature at a rate of 5 °C/min.

The purity and the formation of the desired phase were monitored for crushed and thermally annealed sintered samples by powder X-ray diffraction (XRD; D8 Advance, Bruker, Germany) using $CuK\alpha_1$ radiation and an inductively coupled-plasma (ICP) spectroscopy. As consistent with our previous report,[27] ICP analysis revealed that the composition of sintered 0CuO has no deviation from that intended within the resolution limit. For the XRD, strain-free silicon standard powder (640C, NIST, Gaithersburg, U.S.A.) was used as an internal standard. The instrumental broadening and zero shift were corrected from a profile fitting for patterns of the standard silicon powder. Diffraction patterns were refined using the software package Fullprof software.[28] Refined lattice parameters were converted to the corresponding values for a basic perovskite unit cell using crystallographic relations. For the microstructure analyses, scanning electron microscopy (SEM, XL 30 FEG, Philips, Netherlands) equipped with TSL EBSD system was used on cross-sectioned surfaces of sintered specimens mirror-polished and thermally etched at 900–1000 °C for 30 min depending on the compositions. Stereological interpretation based on the linear intercept technique was used for the determination of size distribution and average grain size.

All samples were ground on both sides to remove the surface regions and electroded with a silver paint. For the temperature-dependent permittivity measurements, the electrodes were first fired at 550 °C for 30 min. Poling was achieved using two successive unipolar cycles at 8 kV/mm at the frequency of 50 mHz at room temperature. Permittivity values together with loss tangent were measured both on poled and unpoled samples, using an impedance analyzer (HP 4192A, Pala Alto, U.S.A.) in the frequency range of 100 Hz–1 MHz and in the temperature range of 25–350 °C. The mechanical quality factor, which has been

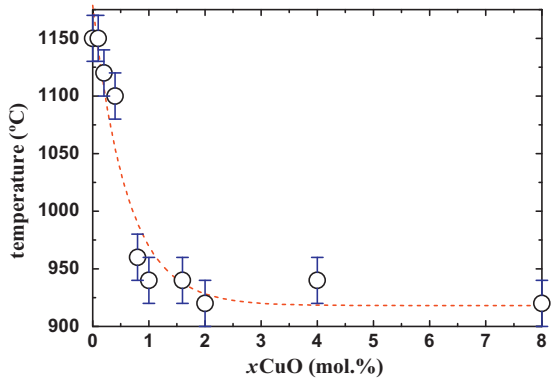

Fig. 1. The temperature required for achieving >98% theoretical density as a function of CuO addition. It is noted that more than 1 mol.% CuO addition leads to a drastic decrease in the sintering temperature. The red broken line is given for an eye guide. (For interpretation of the references to color in this figure legend, the reader is referred to the web version of the article.)

considered one of the most important parameters for checking so-called 'hardening effect', and planar coupling coefficient were measured by a resonance/antiresonance technique.

The strain and polarization hysteresis loops were measured on disc-shaped fresh samples electroded with silver paint, using a Sawyer-Tower circuit equipped with a linear variable differential transformer (LVDT) attached. All the samples were thermally annealed before the measurements. A triangular-shaped wave form with field amplitude of 8 kV/mm at a frequency of 50 mHz was used for the entire measurement as in previous work.[17–20] The small signal d_{33} values were evaluated using Berlincourt meter (YE 2730, SINOCERA).

In order to check for diffusion of Cu^{2+} ions into the lattice and their exact position in the lattice, *X*-band (9.46 GHz) electron paramagnetic resonance (EPR) measurements were carried out using a Bruker EMX 300E spectrometer with a rectangular TE_{112} resonator (Bruker, Germany). The magnetic field was read out with a nuclear magnetic resonance gaussmeter (ER 035M, Bruker, Germany). As a standard field marker, polycrystalline 2,2-diphenyl-1-picrylhydrazyl with $g = 2.0036$ was used for the exact determination of the resonance magnetic field values.

3. Results

3.1. Microstructure

Fig. 1 sums up the changes in a required sintering temperature to obtain ~98% theoretical density as a function of CuO content. Within the experimental error range, little effect of CuO as a sintering additive was noted up to 0.1 mol.% CuO. However, it is seen that the effect of CuO is so pronounced that the sintering temperature drops drastically down below 1000 °C even with the very small addition of 0.8 mol.% CuO, and further increase in CuO content makes the sintering temperature asymptotically approach a temperature as low as 930 °C.

The phase purity and structure were determined by XRD. No trace of secondary phases was detected within the resolution limit of the apparatus, and the structure of all the compositions studied revealed a perovskite structure without any obvious long-range non-cubic distortion, as is consistent with the previous works.[22,27] The XRD patterns of the samples sintered at low temperatures and those sintered at 1150 °C are presented for a selected angular range covering two important reflections, *i.e.* (1 1 1)pc (pc denotes 'pseudocubic' throughout the context) and (2 0 0)pc, in Fig. 2(a) and (b), respectively. Despite the absence of apparent non-cubic distortions, it is evident that the addition of CuO influences crystal structure of all the systems under consideration, which becomes obvious for 8.0CuL and 8.0CuH from the appearance of the superlattice reflection of the rhombohedral 1/2(3 1 1)pc.[29] At the current stage, it is not clearly understood why the superlattice 1/2(3 1 1)pc suddenly appears only in 8.0CuL and 8.0CuH. This could be either due to insufficient intensity for the reflection or due to a structural frustration by the presence of a notable amount of tetragonal symmetry in the compositions except 8.0 mol.% added specimens. A clarification of the issue seems available with a neutron diffraction study as a part of future investigations.

Structural refinement was performed for all the compositions investigated, and the results are presented in Fig. 3(a) and (b). All the profiles were best-fit by assuming a two-phase mixture of rhombohedral *R*3*c* and tetragonal *P*4*bm*. As is consistent with our previous studies,[18,22] 0CuH specimen consisted mostly of tetragonal phase (>90% in volume fraction) with a very small tetragonality of 1.0009. On the introduction of a small amount of CuO, the tetragonality was seen to increase drastically with an increase in the volume fraction of rhombohedral phase. Further increase in the CuO content results in a continuous decrease in the tetragonality which saturates at ~1.002 when $x > 0.8$, while the volume fraction of rhombohedral phase keeps increasing until it reaches ~30%. These results suggest that the solubility limit of CuO into the lattice of BNT–BT–KNN system is about 0.8 mol.%. On the other hand, no significant change in the rhombohedral lattice was denoted.

The microstructures for selected compositions are shown in Fig. 4(a)–(f). As is consistent with the XRD data, no secondary phase is observed within the resolution limit. Considering the fact that the estimated solubility limit of CuO is rather small at about 0.8 mol.%, the absence of detectable secondary phases even with 8.0 mol.% of excess CuO clearly indicates that the residual CuO that is not incorporated into the lattice should form neither a crystalline phase nor a sizable mass. Therefore, it is thought that excessively added CuO could exist in the form of a thin amorphous intergranular phase, which cannot be detected by XRD and is removed mostly during etching process prior to microstructure observation. This conjecture is further supported by a series of microstructural features indicating CuO promotes a liquid phase sintering as will be discussed in details hereafter. The grain size distribution for selected compositions is presented in Fig. 5(a)–(f). The distribution was plotted in two different ways. One is based on conventional stereological technique (represented by black squares), and the other results from the stereological analysis weighted by the corresponding grain size. Thus, the latter indicates the development of a bimodal size distribution more clearly.

It is seen that 0CuH shows a very fine and homogeneous microstructure, also reflected by the distribution plot provided

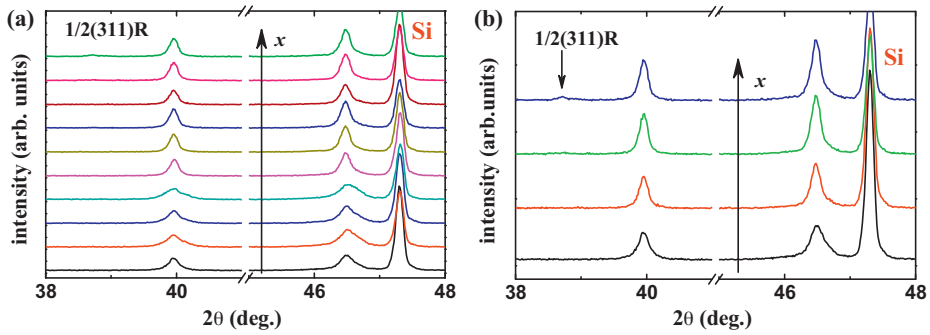

Fig. 2. XRD patterns of the samples sintered at (a) low temperatures and those at (b) 1150 °C. The identity of the profiles is (a) 0CuH, 0.1CuH, 0.2CuL, 0.4CuL, 0.8CuL, 1.0CuL, 1.6CuL, 2.0CuL, 4.0CuL, 8.0CuL and (b) 0CuH, 2.0CuH, 4.0CuH, 8.0CuH from the bottom. A specific angular range is chosen to show (1 1 1)pc and (2 0 0)pc reflections more clearly. The arrows point the direction of increasing CuO amount and the large intensity reflection at the higher angular region is (2 0 0) reflection of the standard silicon powder used.

in Fig. 5(a). With the addition of 0.1 mol.% of CuO, however, the homogeneity of the microstructure tends to be disrupted with the overall grain size increased. Note that the average grain size doubles as compared to that of 0CuH. The changes mentioned are clearly evidenced by the distribution plot presented in Fig. 5(b). Not only the average grain size but also the FWHM are significantly increased. The extent of the bimodality, which is a signature for abnormal grain growth, cannot be discerned from the distribution plot. The abnormal growth is evidenced by the negative grain boundary curvature,[30–32] as marked with an arrow (Fig. 4(b)). It is known that the negative grain boundary curvature causes the observed grains larger than the average to eventually grow abnormally, as manifested by a solid-state single crystal growth technique.[33] In addition, trapped small grains (marked with a circle) are frequently observed in this type of grain.[31,34,35]

Neither significant difference in the microstructure nor any systematic dependence of the microstructure on the amount of CuO added was noted up to the concentration level of ~1 mol.%. Once the addition level of CuO exceeds ~1 mol.%, however, significantly large grains with rather well-developed facets start to appear. The average size of the matrix grains tends to be smaller. Here again, though the effect of the CuO addition is overall evidently clear, no systematic correlation was discerned between the CuO concentration and the parameters characterizing microstructure such as average grain size. The presence of the facets suggests that the appearance of the abnormally grown grains is a consequence of liquid-phase sintering of faceted grains.[30,35,36]

A distinctive morphological feature is related to the large abnormally grown grains (see Fig. 4(c) for example). The large grains are actually composed of two grains interweaved with each other and often with many smaller grains trapped inside. EBSD analysis on representative large abnormal grains as presented in Fig. 6 demonstrates that the interweaving feature is due to Σ3 coincidence site lattice (CSL) relationship, also termed a crystallographic twin. The interfaces are indicated by thick black lines. It has been reported that the abnormally grown grains with perovskite structure often have this feature.[34,35,37–39] The interweaving feature of the currently observed twin is often called the 'penetration twin' since the compositional plane that actually separates the two twinned domains interpenetrates the crystallographic twin plane. It was demonstrated that the growth advantage due to the presence of the penetration twin is given by the presence of never vanishing reentrant edges originating from a zigzag-shaped twin boundary.[38,40] Smaller grains are both partially and fully trapped inside a large grain and the large grain is found to form either a low-angle relation (indicated by white lines) or some special misorientation like Σ9 (indicated by yellow lines)[37] that occurs between two domains sharing another domain in common with a Σ3 CSL relation. The criterion for the low-angle was set to be the misorientation angle less than 8°. Note that low angle grain boundaries provide preferential sites for 2-dimensional nucleation in the presence of liquid phase and potentially lead to abnormal grain growth, which was explained as the grain boundary reentrant edge (GBRE) mechanism.[34,35]

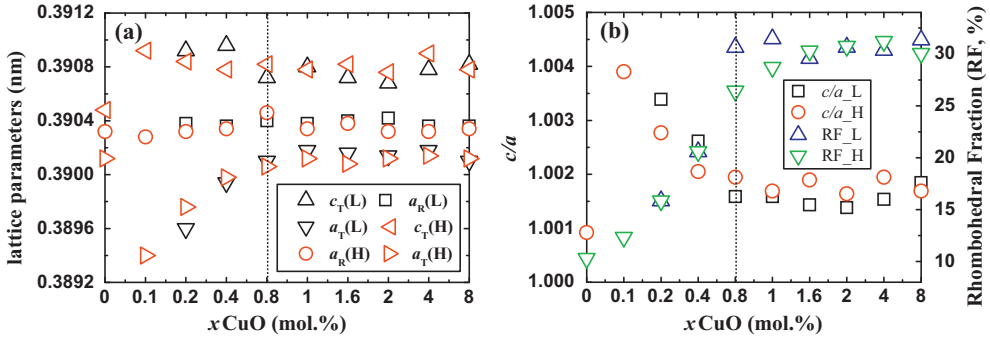

Fig. 3. Changes in (a) the lattice parameters and (b) tetragonality as a function of CuO content. No notable change in both the lattice parameters and tetragonality is discerned above $x = 0.8$.

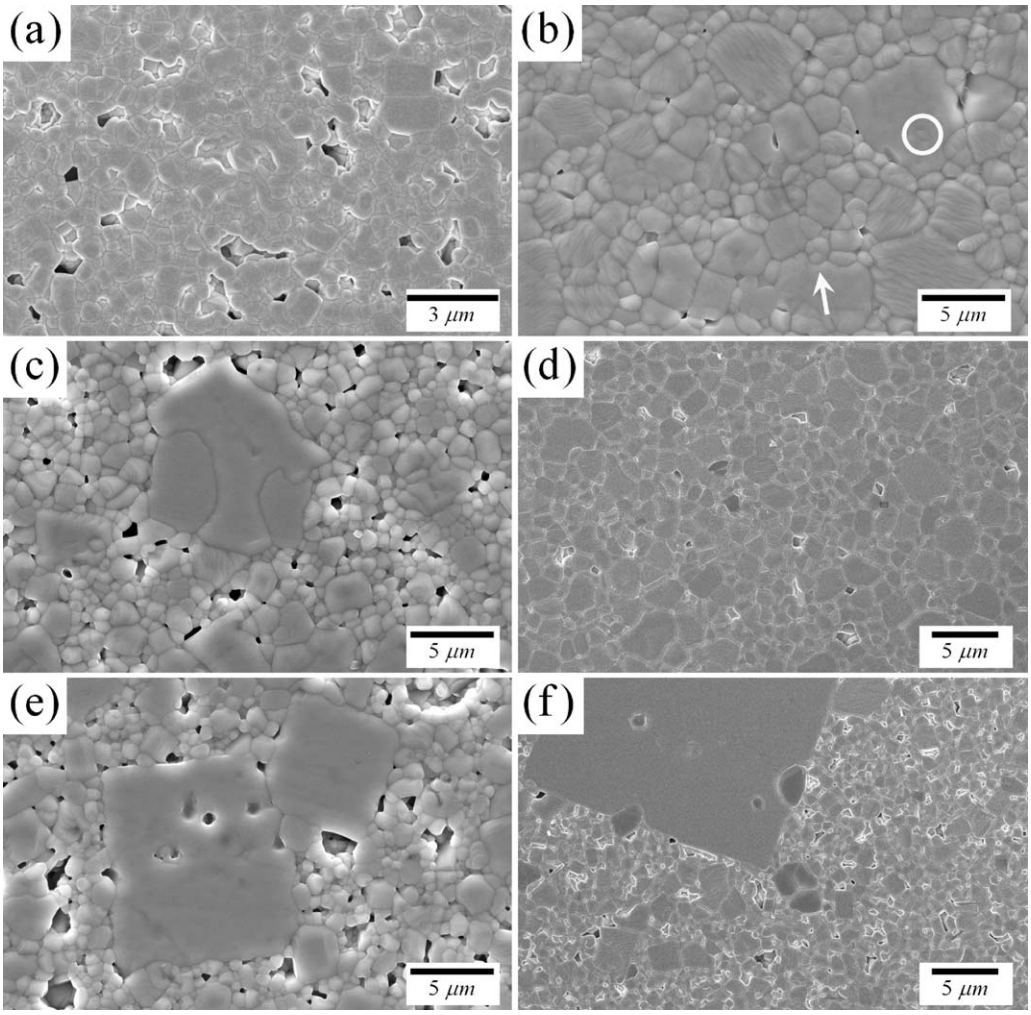

Fig. 4. Polished and thermally etched microstructure of (a) 0CuH (0CuL), (b) 0.1CuH (0.1CuL), (c) 2.0CuL, (d) 2.0CuH, (e) 8.0CuL, and (f) 8.0CuH.

3.2. Electrical properties

Temperature dependent dielectric permittivity and the corresponding loss factor for the poled materials were measured from room temperature to 350 °C. Spectra of the selected compositions are presented in Fig. 7. All the samples exhibit the permittivity peak at ~250 °C, which is known to be related to a transition to a high temperature paraelectric phase.[4,19] Other transitions near ~150 °C and ~50 °C are clearly indicated in the case of 0.1CuH (Fig. 7(b)), most strongly, in 0CuH (Fig. 7(a)), and mildly in 0.1CuH (Fig. 7(d)) by the shoulders in the permittivity curves. The transitions are also accompanied by the anomalous behavior in loss tangents.

It can be concluded that the transition at ~250 °C to a high temperature paraelectric phase exhibits practically no frequency dispersion as indicated in Fig. 7(b) for 0.1CuH sample. Apparent dispersions indicated in other specimens can be attributed to the space charge polarization from the increased dc conductivity. This is represented by the large loss tangent values in Fig. 7. While 0.1 mol.% CuO increases the sample resistance, higher amount of CuO addition decreases the sample resistance substantially.

The anomaly at ~150 °C exhibits strong frequency dispersion, which has been taken as an indicator that the BNT-based materials are relaxors.[41,42] The other anomaly happens at a higher temperature (~250 °C), which is known to be related to a transition to a high temperature paraelectric phase.[4,19] In the case of 0CuH and 0.1CuH, both permittivity and loss tangent exhibit an additional anomaly near ~50 °C. This temperature was commonly defined as a depolarization temperature[4,43] and is characterized by a frequency-independent sharp peak in loss tangent. An important feature to be noted is that a sharp discontinuity (see Fig. 7(a) and (b)) in the dielectric permittivity and loss are only visible in the specimens, where $x = 0$ or 0.001.

The strain and polarization hysteresis loops were measured on unpoled fresh samples, and presented in Fig. 8(a) and (b) for selected compositions. All the polarization loops are well-saturated at 8 kV/mm. With the addition of CuO, no significant change in the maximum strain and polarization values is discerned, while the corresponding remanent values change drastically. Even at the addition level of 0.1 mol.%, both remanent strain and polarization values increase sharply. In the meantime, the highly constricted polarization hysteresis loop of 0CuH tends to depinch. However, a further increase

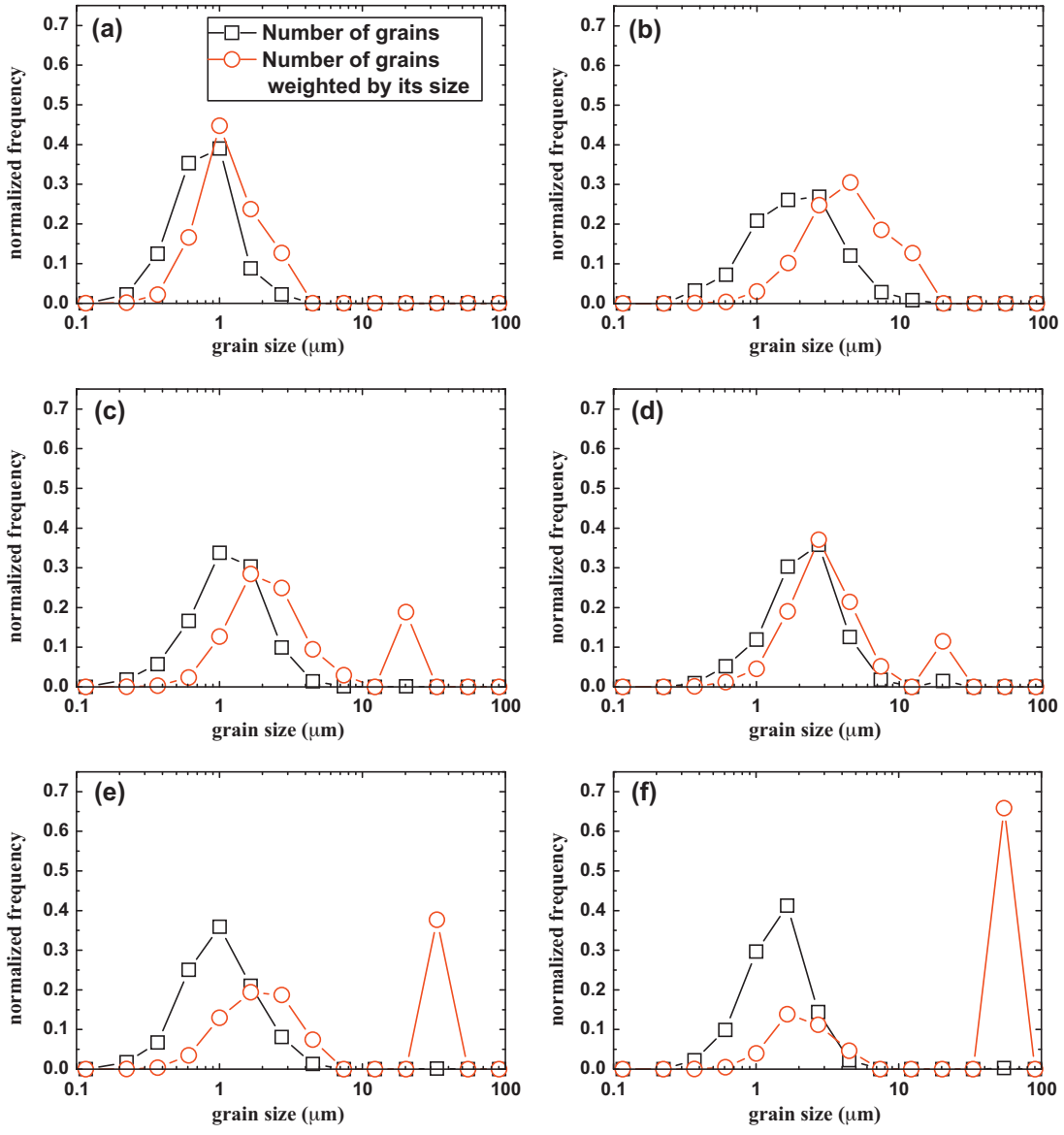

Fig. 5. Grain size distribution of the microstructure of (a) 0CuH, (b) 0.1CuH, (c) 2.0CuL, (d) 2.0CuH, (e) 8.0CuL, and (f) 8.0CuH.

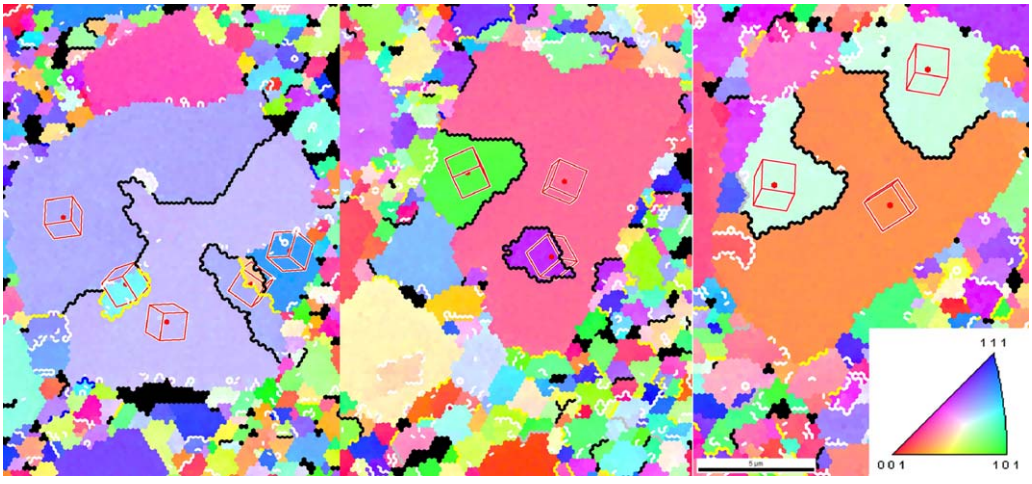

Fig. 6. EBSD images on the microstructures containing representative abnormally grown grains in CuO-added specimens. The interfaces marked black and white represent Σ3 and low-angle relations, which make the majority. The scale bar at the bottom right denotes 5 μm in length.

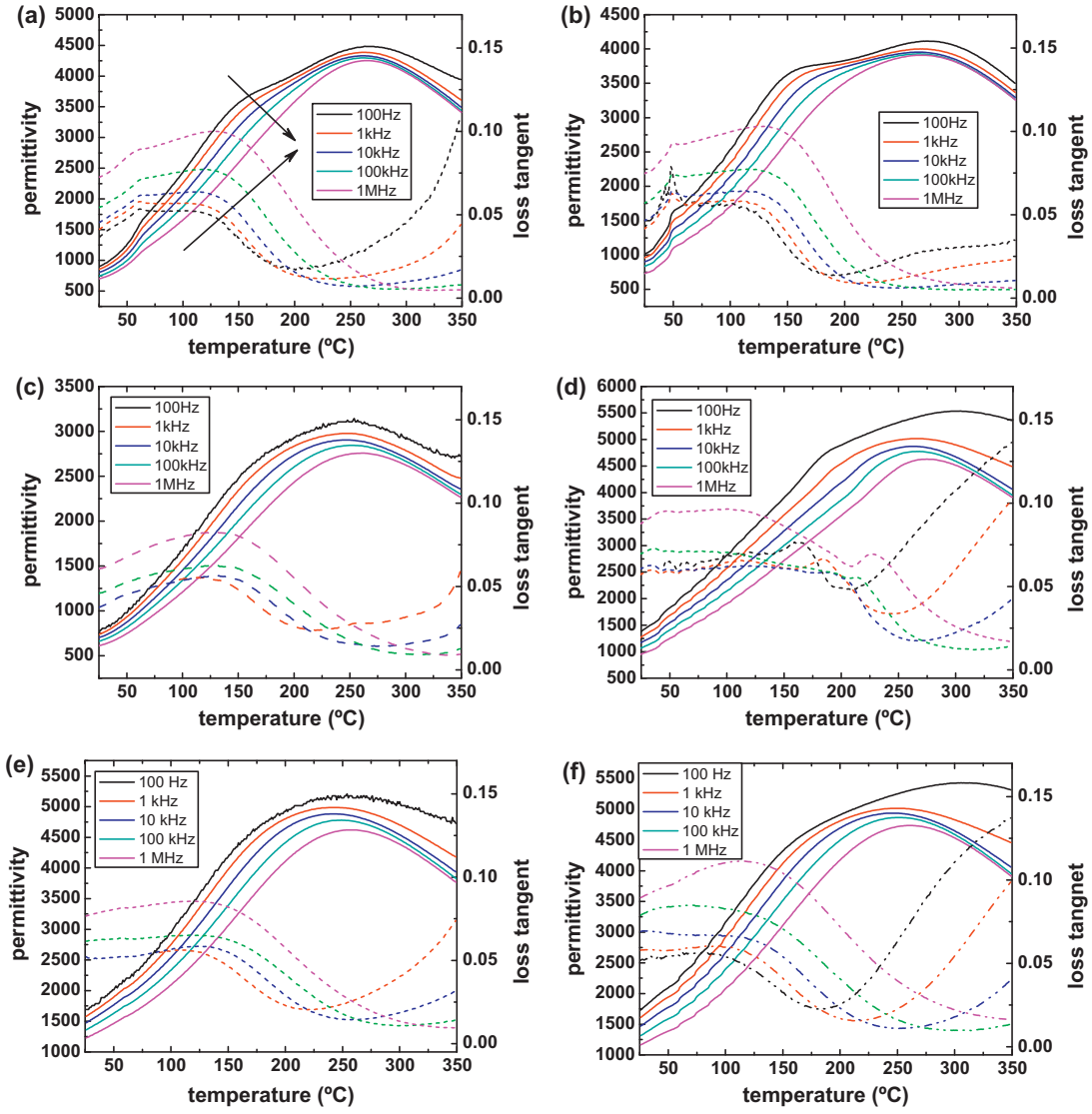

Fig. 7. Temperature dependent permittivity with corresponding loss tangent measured on (a) 0CuH, (b) 0.1CuH, (c) 2.0CuL, (d) 8.0CuL, (e) 2.0CuH, and (f) 8.0CuH, poled at 8 kV/mm at room temperature. Arrows point in direction of increasing frequency.

in the amount of CuO rather reduces this effect. Both remanent strain and polarization decrease slightly. It seems that the sudden increase and decrease in the remanent strain and polarization, respectively, indicates a rather small solubility limit of Cu^{2+} for the system and is a consequence of the disappearance of the 'weakly' ferroelectric phase by the introduction of CuO, as evidenced by the X-ray diffraction study.

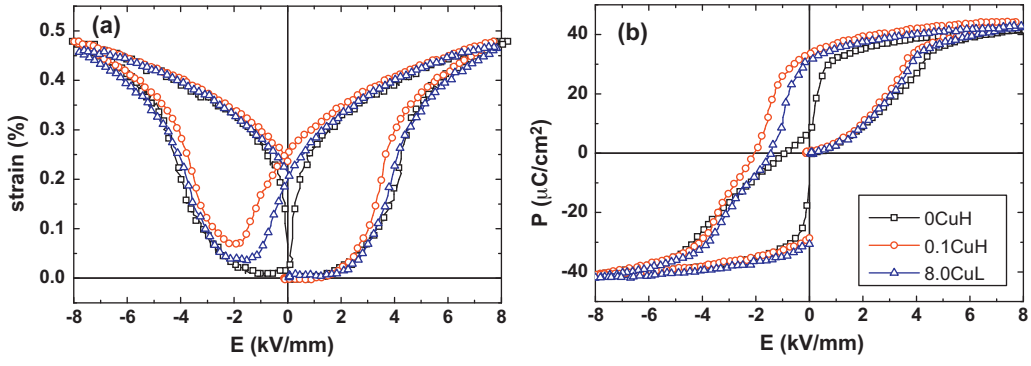

Fig. 8. Strain and polarization hysteresis loops for selected compositions during poling cycle.

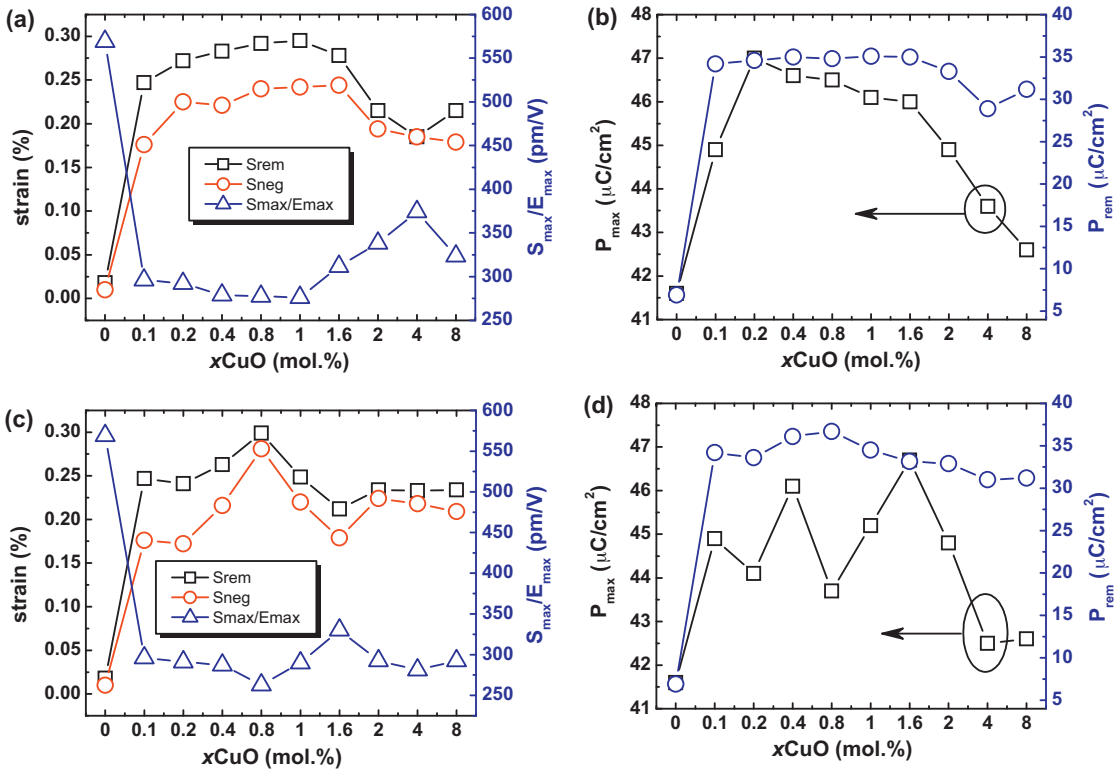

Fig. 9. Changes in the characteristic parameters collected from (a) strain and (b) polarization hysteresis loops of the samples sintered at lower temperatures as well as those from (c) strain and (d) polarization loops of the specimens sintered at 1150 °C.

The characteristic parameters from the strain and polarization hysteresis loops for all the specimens prepared and tested are summarized in Fig. 9. The coercive field was excluded from the list of the characteristic parameters, because the polarization hysteresis loops of all the specimens of the current investigation exhibit a trace of a constriction that indicates the presence of a phase transition, as evidenced in Fig. 8. It is seen that the most drastic change in all properties takes place between 0CuH and 0.1CuH. In all cases, both negative and remanent strains as well as remanent polarization increase sharply, indicating that a ferroelectric order is induced. Due to the increase in the remanent strain with the maximum strain maintained, the large signal d_{33} (S_{max}/E_{max}), which is a figure of merit for actuator operated in a unipolar mode, is seen to decrease significantly. Note that S_{max}/E_{max} is given by the difference between the maximum and remanent strains normalized by the applied electric field, and therefore, an increase in the remanent strain due to the presence of stable ferroelectric order on removal of electric field results in a significant decrease in unipolar actuating performance.[20]

On the other hand, no clear dependence of the parameters of either 100*x*CuH or 100*x*CuL on the amount of CuO is denoted with a further increase of CuO addition. Further, no correlation is observed even between sintering temperature and properties. The absence of a systematic dependence of sintering conditions and properties on the amount of CuO addition could be attributed to the uncontrolled amount of CuO diffusing into the lattice and the inhomogeneous microstructure resulting from abnormal grain growth. Nevertheless, it is apparent that the addition of CuO favors a ferroelectric order, characterized by the development of remanent strain and polarization.

The d_{33} values of 100*x*CuH and 100*x*CuL after being poled at room temperature were measured and compared in Fig. 10. Consistent with our previous reports,[17,20,27] the poling treatment is not as effective for 0CuH with the d_{33} value as small as ~20 pC/N. However, once CuO is introduced into the system, the d_{33} values increase and fall into a band between 160 and 200 pC/N. It is interesting to see that the d_{33} values of 100*x*CuH are higher than those of 100*x*CuL for all compositions studied. This is suggested to be related to the extrinsic contributions of the piezoelectric coefficient, which are enhanced with larger grain

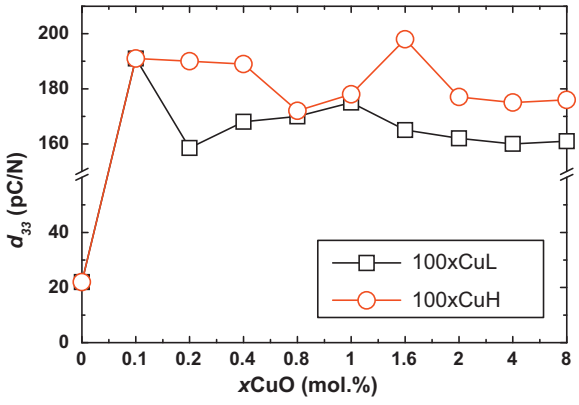

Fig. 10. Summary of the piezoelectric coefficient d_{33} as a function of composition.

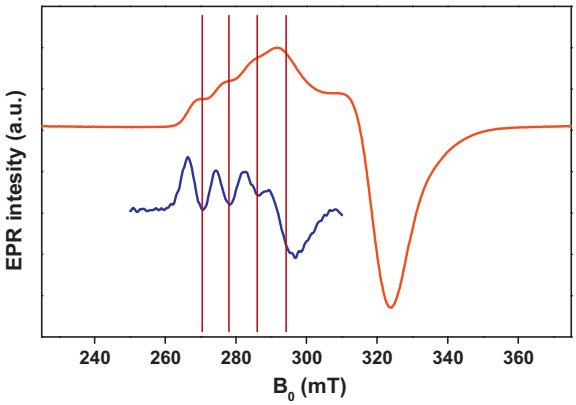

Fig. 11. X-band (9.4 GHz) EPR spectra of CuO-doped 92BNT–6BT–2KNN at 20 K. The second curve represents the numerical derivative of the experimental spectrum in the g_{zz}-region together with a 'stick-spectrum' indicating the quartet ^{63}Cu-hyperfine splitting.

size.[44] Since one of the most prominent effects of acceptor doping in perovskite piezoceramics is a significant increase in the mechanical quality factor (Q_m) and a decrease in the coupling factor (k_p), the change in the Q_m and k_p as a function of CuO content was monitored. Contrary to the expectation, both Q_m and k_p were increased, though the increase is marginal. The Q_m value was slightly increased from 93 for 0CuH to 123 for 0.8CuH and then leveled at ~110 with a further increase in CuO content. The k_p value was also increased from 0.18 for 0CuH to 0.25 for 0.8CuH and then leveled at ~0.21. This rather counterintuitive result may be due to the fact that a noticeable ferroelectric order is only induced with the addition of CuO.[20]

Further insight into the role of CuO could be gained using EPR spectroscopy[45] to a 2.0CuL specimen (Fig. 11). The EPR-spectrum is characteristic for the Cu^{2+}-charge state in octahedral coordination.[46] However, the resonances are considerably broadened such that the Cu^{2+} spin-Hamiltonian parameters needed for a defect-structural analysis are not directly accessible. Therefore, a numerical derivative of the g_{zz}-region of the spectrum was analyzed instead, which in principal corresponds to a second-harmonic-generated detection scheme.[47] The quartet ^{63}Cu-hyperfine splitting is indicated by 'stick-spectrum' and the corresponding g_{zz}-value is taken as the center between the second and third hyperfine line. Furthermore, by applying a recently developed semi-empirical scheme,[48] the formation of a $(Cu''_{Ti} - V_O^{\bullet\bullet})^{\times}$ defect complex is obtained, similar to the situation in CuO-doped $PbTiO_3$.[49] Because the resulting defect complex is electrically neutral, it has no impact on the concentration of other intrinsically present defects in this compound such as cation or anion vacancies for instance. On the other hand, the existence of $(Cu''_{Ti} - V_O^{\bullet\bullet})^{\times}$ defect dipoles, which exhibit a marked defect polarization,[50] provide a means to explain the observed induced ferroelectric order in the polarization and strain hysteresis loops as function of CuO doping.

4. Discussion

It is demonstrated that CuO, as a sintering aid, induces significant changes both in the microstructure and in the electrical properties in the system. The most pronounced effect of the CuO addition lies in the stabilization of a ferroelectric order in the 0.92BNT–0.06BT–0.02KNN ceramic. This is evident specifically from Fig. 8 with significant remanent strain and polarization after poling. The loss of remanent strain and polarization in 0.92BNT–0.06BT–0.02KNN was ascribed to the presence of a 'weakly' ferroelectric phase at zero field which transforms reversibly into a nominal ferroelectric *R*3*c* phase.[20,22] The observed stabilization of a 'strongly' ferroelectric order indicates that the CuO addition negates the possibility of a reversible transformation from 'weakly' ferroelectric to normal ferroelectric. Hence, the CuO additions into BNT–BT–KNN bring back room temperature properties related to the original BNT–BT ceramic.[17]

This view can be better supported with an inclusion of the structural knowledge obtained. Firstly, with the addition of CuO, the crystal structure of the system changes from *P*4*bm* into a mixture of *P*4*bm* and *R*3*c*, and then into dominantly *R*3*c* phase. Note that this series of phase transitions also occurs in 0CuH during electrical poling.[22] Secondly, though less pronounced, a trace of pinching in the polarization hysteresis persists even in the CuO-added systems. This implies that though small in extent, the 'weakly' ferroelectric *P*4*bm* phase still exists in all the systems investigated, and thus the presence of the electric-field-induced phase transition is not excluded. Here, the lack of the electric-field-induced phase transition does not necessarily mean that the addition of CuO simply shifts the phase transition temperature between *R*3*c* and *P*4*bm* upwards. As shown in Fig. 7, a clear distinction in the temperature-dependent dielectric permittivity and loss develops with the addition of CuO. A sharp discontinuity normally assigned as a depolarization temperature is no longer observed in CuO-added systems once the addition level exceeds 0.1 mol.%. In the meantime, the first dielectric anomaly represented as a 'shoulder' tends to disappear, which implies that CuO not only influences the room temperature phase stability but also the propensity of the polymorphism of the system. However, to have a detailed and exact picture on this issue, more elaborate and systematic investigations are required.

As demonstrated by EPR spectroscopy, Cu^{2+} ions added in the form of CuO diffuse into the lattice and replace the B-site ions, forming a defect dipole associated with the charge balancing oxygen vacancy. This result is further supported by the microstructural aspect. Again, the fact that the addition of CuO affects the phase stability 0.92BNT–0.06BT–0.02KNN favoring the rhombohedral over the tetragonal symmetry clearly indicates that Cu^{2+} diffuses into the lattice. With respect to the ionic size of Cu^{2+} (0.73 Å),[51] Cu^{2+} is expected to replace most likely B-site ions such as Ti^{4+} or Nb^{5+}, though it can substitute both A-site ions with 12-fold coordination and B-site ions with 6-fold coordination. This assumption is also strongly supported by the following two arguments. One is the well-known tolerance factor (t) concept and the other the appearance of penetration twinned abnormal grains. According to an empirical indication from the tolerance factor, it is known that a high symmetry phase such as a cubic or a tetragonal is usually found when $t > 1$, while the lower phase symmetries such as orthorhombic, monoclinic, or rhombohedral are often found when $t < 1$.[5] In fact, the sub-

stitution of Cu^{2+} (0.73 Å) either for Ti^{4+} (0.61 Å) or for Nb^{5+} (0.64 Å) leads to a decrease in the tolerance factor, and thus a lower symmetry phase is favored. On the other hand, another supporting argument for the substitution site of Cu^{2+} is the fact that most abnormal grains investigated on CuO added specimens show the penetration twin characteristic, the formation of which is known to be facilitated when the electrical charge distribution in B-site is disturbed.[34]

5. Conclusions

0.92BNT–0.06BT–0.02KNN lead-free piezoceramics were successfully sintered at temperatures as low as ~930 °C with CuO as a sintering additive. However, the reduction in the sintering temperature was accompanied by abnormal grain growth. Based on the SEM analysis combined with EBSD, it was suggested that the reduction in the sintering temperature and the appearance of the abnormal grain growth are due to the formation of a liquid phase. In addition, XRD and microstructure analyses showed that CuO not only promotes the formation of a liquid phase but also induces a phase transition by substituting for B-site elements such as Ti^{4+} or Nb^{5+}. Dielectric permittivity and loss showed that with CuO addition, the frequency-independent sharp anomaly, normally referred to as 'depolarization' temperature, disappears. Polarization and strain hysteresis loops measured at room temperature clearly demonstrated that a 'strongly' ferroelectric order is induced with CuO. It was proposed that the induced ferroelectric order is largely attributed to Cu^{2+} ions diffusing into the crystal lattice, which form $(Cu''_{Ti} - V_O^{\bullet\bullet})^{\times}$ defect dipoles. The presence of such strongly associated defect dipole was confirmed by EPR spectroscopy. The current results imply that a successful utilization of CuO as a low-temperature sintering aid could be accompanied by the introduction of a donor element that may nullify the effect of Cu^{2+} as an acceptor.

Acknowledgements

This work was financially supported by the state center ADRIA on adaptronics and by SFB 595. The work was also supported by the Korea Research Foundation through KRF-2008-314-D00174 and KRF-2007-331-D00195.

References

1. Goosey M. An overview of the current status of lead-free assembly and related issues. *Circuit World* 2003;**29**:23–7.
2. O'Neil A, JWatkins JJ. Green chemistry in the microelectronics industry. *Green Chem* 2004;**6**:363–8.
3. Shrout TR, Zhang SJ. Lead-free piezoelectric ceramics: alternatives for PZT? *J Electroceram* 2007;**19**:113–26.
4. Takenaka T, Nagata H, Hiruma Y. Current developments and prospective of lead-free piezoelectric ceramics. *Jpn J Appl Phys* 2008;**47**:3787–801.
5. Rödel J, Jo W, Seifert KTP, Anton EM, Granzow T, Damjanovic D. Perspective on the development of lead-free piezoceramics. *J Am Ceram Soc* 2009;**92**:1153–77.
6. Panda PK. Review: environmental friendly lead-free piezoelectric materials. *J Mater Sci* 2009;**44**:5049–62.
7. Chawla N. Thermomechanical behaviour of environmentally benign Pb-free solders. *Int Mater Rev* 2009;**54**:368–84.
8. Rödel J, Kounga ABN, Weissenberger-Eibl M, Koch D, Bierwisch A, Rossner W, et al. Development of a roadmap for advanced ceramics: 2010–2025. *J Eur Ceram Soc* 2009;**29**:1549–60.
9. Takenaka T, Maruyama K-I, Sakata K. $(Bi_{1/2}Na_{1/2})TiO_3$–$BaTiO_3$ system for lead-free piezoelectric ceramics. *Jpn J Appl Phys* 1991;**30**:2236–9.
10. Saito Y, Takao H, Tani T, Nonoyama T, Takatori K, Homma T, et al. Lead-free piezoceramics. *Nature* 2004;**432**:84–7.
11. Randall CA, Kelnberger A, Yang GY, Eitel RE, Shrout T. High strain piezoelectric multilayer actuators – a material science and engineering challenge. *J Electroceram* 2005;**14**:177–91.
12. Donnelly NJ, Shrout TR, Randall CA, Reaney IM. Thermodynamic reactions between PZT and Ag/Pd powders: relevance to cofiring of multilayer actuators. *J Am Ceram Soc* 2008;**91**:1013–8.
13. Schütz D, Krauss W, Albering J, Kurta C, Reichmann K. The chemical interaction of silver–palladium alloy electrodes with bismuth-based piezomaterials. *J Am Ceram Soc* 2010;**93**:1142–7.
14. Matsubara M, Yamaguchi T, Kikuta K, Hirano S. Sinterability and piezoelectric properties of (K, Na)NbO_3 ceramics with novel sintering aid. *Jpn J Appl Phys* 2004;**43**:7159–63.
15. Park H-Y, Choi J-Y, Choi M-K, Cho K-H, Nahm S, Lee H-G, et al. Effect of CuO on the sintering temperature and piezoelectric properties of $(Na_{0.5}K_{0.5})NbO_3$ lead-free piezoelectric ceramics. *J Am Ceram Soc* 2008;**91**:2374–7.
16. Eichel R-A, Erünal E, Drahus MD, Smyth DM, Tol Jv, Acker J, et al. Local variations in defect polarization and covalent bonding in ferroelectric Cu^{2+}-doped PZT and KNN functional ceramics at the morphotropic phase boundary. *Phys Chem Chem Phys* 2009;**11**:8698–705.
17. Zhang S-T, Kounga AB, Aulbach E, Ehrenberg H, Rödel J. Giant strain in lead-free piezoceramics $Bi_{0.5}Na_{0.5}TiO_3$–$BaTiO_3$–$K_{0.5}Na_{0.5}NbO_3$ system. *Appl Phys Lett* 2007;**91**, 112903:3pp.
18. Zhang S-T, Kounga AB, Aulbach E, Granzow T, Jo W, Kleebe H-J, et al. Lead-free piezoceramics with giant strain in the system $Bi_{0.5}Na_{0.5}TiO_3$–$BaTiO_3$–$K_{0.5}Na_{0.5}NbO_3$. Part I. Structure and room temperature properties. *J Appl Phys* 2008;**103**, 034107:8pp.
19. Zhang S-T, Kounga AB, Aulbach E, Jo W, Granzow T, Ehrenberg H, et al. Lead-free piezoceramics with giant strain in the system $Bi_{0.5}Na_{0.5}TiO_3$–$BaTiO_3$–$K_{0.5}Na_{0.5}NbO_3$. Part II. Temperature dependent properties. *J Appl Phys* 2008;**103**, 034107:7pp.
20. Jo W, Granzow T, Aulbach E, Rödel J, Damjanovic D. Origin of the large strain response in $(K_{0.5}Na_{0.5})NbO_3$-modified $(Bi_{0.5}Na_{0.5})TiO_3$–$BaTiO_3$ lead-free piezoceramics. *J Appl Phys* 2009;**105**, 094102:5pp.
21. Kling J, Tan X, Jo W, Kleebe H-J, Fuess H, Rödel J. *In situ* transmission electron microscopy of electric field-triggered reversible domain formation in Bi-based lead-free piezoceramics. *J Am Ceram Soc* 2010;**93**:2452–5.
22. Hinterstein M, Knapp M, Hölzel M, Jo W, Cervellino A, Ehrenberg H, et al. Field-induced phase transition in $Bi_{1/2}Na_{1/2}TiO_3$-based lead-free piezoelectric ceramics. *J Appl Cryst* 2010;**43**:1314–21.
23. Webber KG, Zhang Y, Jo W, Daniels JE, Rödel J. High temperature stress-induced "double looplike" phase transitions in Bi-based perovskites. *J Appl Phys* 2010;**108**, 014101:6pp.
24. Eichel R-A. Defect structure of oxide ferroelectrics – valence state, site of incorporation, mechanisms of charge compensation and internal bias fields. *J Electroceram* 2007;**19**:9–21.
25. Lin D, Kwok KW, Chan HLW. Double hysteresis loop in Cu-doped $K_{0.5}Na_{0.5}NbO_3$ lead-free piezoelectric ceramics. *Appl Phys Lett* 2007;**90**:232903–13.
26. Hagh NM, Kerman K, Jadidian B, Safari A. Dielectric and piezoelectric properties of Cu^{2+}-doped alkali niobates. *J Eur Ceram Soc* 2009;**29**:2325–32.
27. Jo W, Erdem E, Eichel R-A, Glaum J, Granzow T, Damjanovic D, et al. Effect of Nb-donor and Fe-acceptor in $(Bi_{1/2}Na_{1/2})TiO_3$–$BaTiO_3$–$(K_{0.5}Na_{0.5})NbO_3$ lead-free piezoceramics. *J Appl Phys* 2010;**108**, 014110:6pp.
28. Roisnel T, Rodriguez-Carvajal J. WinPLOTR: a windows tool for powder diffraction pattern analysis. *Mater Sci Forum* 2001;**378-3**:118–23.

29. Guo R, Cross LE, Park S-E, Noheda B, Cox DE, Shirane G. Origin of the high piezoelectric response in $PbZr_{1-x}Ti_xO_3$. *Phys Rev Lett* 2000;**84**:5423–6.
30. Jung Y-I, Yoon DY, Kang S-JL. Coarsening of polyhedral grains in a liquid matrix. *J Mater Res* 2009;**24**:2949–59.
31. Kang S-JL. *Sintering: densification, grain growth & microstructure*. Oxford: Elsevier; 2005.
32. Rödel J, Glaeser AM. Anisotropy of grain growth in alumina. *J Am Ceram Soc* 1990;**73**:3292–301.
33. Khan AJ, Meschke FA, Li T, Scotch AM, Chan HM, Harmer MP. Growth of PMN:PT single crystals from (1 1 1) substrates by seeded polycrystal conversion. *J Am Ceram Soc* 1999;**82**:2958–62.
34. Jo W, Chung U-J, Hwang N-M, Kim D-Y. Effect of SiO_2 and TiO_2 addition on the morphology of abnormally grown large $Pb(Mg_{1/3}Nb_{2/3})O_3$–35 mol% $PbTiO_3$ grains. *J Am Ceram Soc* 2005;**88**:1992–4.
35. Jo W, Kim D-Y, Hwang N-M. Effect of interface structure on the microstructure evolution of ceramics. *J Am Ceram Soc* 2006;**89**:2369–80.
36. Rohrer GS. Influence of interface anisotropy on grain growth and coarsening. *Annu Rev Mater Res* 2005;**35**:99–126.
37. Jo W, Chung U-J, Hwang N-M, Kim D-Y. Temperature dependence of the coarsening behavior of (Ba, Sr)TiO_3 grains dispersed in a SiO_2-rich liquid matrix. *J Eur Ceram Soc* 2003;**23**:1565–9.
38. Kim K-W, Jo W, Jin H-R, Hwang N-M, Kim D-Y. Abnormal grain growth of lead zirconium titanate (PZT) ceramics induced by the penetration twin. *J Am Ceram Soc* 2006;**89**:1530–3.
39. Schmelz H, Meyer A. The evidence for abnormal grain growth below the eutectic temperature in $BaTiO_3$ Ceramics. *Ber Dtsch Keram Ges* 1982;**59**:436–40.
40. Chung U-J, Jo W, Lee J-H, Hwang N-M, Kim D-Y. Coarsening process of penetration-twinned grains in PMN-35 mol% PT ceramics. *J Am Ceram Soc* 2004;**87**:125–8.
41. Hiruma Y, Nagata H, Takenaka T. Phase diagrams and electrical properties of $(Bi_{1/2}Na_{1/2})TiO_3$-based solid solutions. *J Appl Phys* 2008;**104**, 124106:12pp.
42. Suchanicz J, Kusz J, Bohm H, Duda H, Mercurio JP, Konieczny K. Structural and dielectric properties of $(Na_{0.5}Bi_{0.5})_{0.70}Ba_{0.30}TiO_3$ ceramics. *J Eur Ceram Soc* 2003;**23**:1559–64.
43. Hiruma Y, Nagata H, Takenaka T. Formation of morphotropic phase boundary and electrical properties of $(Bi_{1/2}Na_{1/2})TiO_3$–$Ba(Al_{1/2}Nb_{1/2})O_3$ solid solution ceramics. *Jpn J Appl Phys* 2009;**48**:09KC08-6.
44. Damjanovic D, Demartin M. Contribution of the irreversible displacement of domain walls to the piezoelectric effect in barium titanate and lead zirconate titanate ceramics. *J Phys: Condens Matter* 1997;**9**:4943–53.
45. Eichel R-A. Structural and dynamic properties of oxygen vacancies in perovskite oxides – analysis of defect chemistry by modern multi-frequency and pulsed EPR techniques. *Phys Chem Chem Phys* 2011;**13**: 368–84.
46. Abragam A, Bleaney B. *Electron paramagnetic resonance of transition ions*. Oxford: Clarendon Press; 1970.
47. Poole Jr CP. *Electron spin resonance – a comprehensive treatise on experimental techniques*. New York: Dover Publications; 1983.
48. Eichel R-A, Drahus MD, Jakes P, Erünal E, Erdem E, Parashar SKS, et al. Defect structure and formation of defect complexes in Cu^{2+}-modified metal oxides derived from a spin-Hamiltonian parameter analysis. *Mol Phys* 2009, doi:10.1080/00268970903084920.
49. Eichel R-A, Erhart P, Träskelin P, Albe K, Kungl H, Hoffmann MJ. Defect-dipole formation in copper-doped $PbTiO_3$ ferroelectrics. *Phys Rev Lett* 2008;**100**, 095504:4pp.
50. Neumann H, Arlt G. Dipole orientation in Cr-modified $BaTiO_3$ ceramics. *Ferroelectrics* 1987;**76**:303–10.
51. Shannon RD, Prewitt CT. Effective ionic radii in oxides and fluorides. *Acta Crystallogr B* 1969;**25**:925–46.